



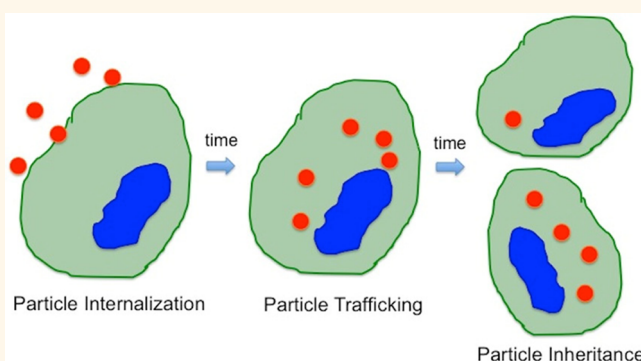
ARRCI
J

Particles on the Move: Intracellular Trafficking and Asymmetric Mitotic Partitioning of Nanoporous Polymer Particles

Yan Yan,^{†,‡} Zon W. Lai,^{‡,§,⊥} Robert J. A. Goode,[‡] Jiwei Cui,[†] Tess Bacic,[†] Marloes M. J. Kamphuis,[†] Edouard C. Nice,^{‡,*} and Frank Caruso^{†,*}

[†]Department of Chemical and Biomolecular Engineering, The University of Melbourne, Parkville, Victoria 3010, Australia, [‡]Department of Biochemistry and Molecular Biology, Monash University, Victoria 3800, Australia, and [§]Institute for Molecular Medicine and Cell Research, University of Freiburg, Freiburg 79104, Germany. [⊥]Y. Yan and Z. W. Lai contributed equally.

ABSTRACT Nanoporous polymer particles (NPPs) prepared by mesoporous silica templating show promise as a new class of versatile drug/gene delivery vehicles owing to their high payload capacity, functionality, and responsiveness. Understanding the cellular dynamics of such particles, including uptake, intracellular trafficking, and distribution, is an important requirement for their development as therapeutic carriers. Herein, we examine the spatiotemporal map of the cellular processing of submicrometer-sized disulfide-bonded poly(methacrylic acid) (PMA_{SH}) NPPs in HeLa cells using both flow cytometry and fluorescence microscopy. The data show that the PMA_{SH} NPPs are transported from the early endosomes to the lysosomes within a few minutes. Upon cell division, the lysosome-enclosed PMA_{SH} NPPs are distributed asymmetrically between two daughter cells. Statistical analysis of cells during cytokinesis suggests that partitioning of particles is biased with an average segregation deviation of 60%. Further, two-dimensional difference gel electrophoresis (2D-DIGE) analysis reveals that 127 out of 3059 identified spots are differentially regulated upon exposure to the PMA_{SH} NPPs. Pathway analysis of the proteomics data suggests that ubiquitylation, a reversible modification of cellular proteins with ubiquitin, plays a central role in overall cellular responses to the particles. These results provide important insights into the cellular dynamics and heterogeneity of NPPs, as well as the mechanisms that regulate the motility of these particles within cells, all of which have important implications for drug susceptibility characteristics in cancer cells using particle-based carriers.



KEYWORDS: mesoporous silica particles · mitotic partitioning · asymmetric division · intracellular fate · proteomics · ubiquitylation

In recent years there has been growing interest in investigating and understanding cellular interactions of nanoengineered particles, as their cellular dynamics can inform key aspects for ensuring safe and effective therapeutic delivery using particle carriers. Previous studies have shown that endocytosis provides a major route for cellular entry and that the lysosomal compartments are the predominant intracellular destination for different types of particles.^{1,2} While current work is heavily focused on mapping endocytic pathways involved in particle internalization,³ the cellular processing beyond lysosomal accumulation

of incoming particles is generally poorly understood.

Traditionally, endocytosis has been regarded simply as a process for ingesting external molecules prior to digesting them, or recycling them back to the cell surface.⁴ More recently, it has become clear that the endocytic systems are intimately connected with other seemingly disparate cell functions, such as cell migration, antigen presentation, and cell division.^{5,6} For example, asymmetric partitioning of endosomes has been observed at the initial cleavage of both the *Caenorhabditis elegans* embryo⁷ and mammalian hematopoietic stem cells.⁸

* Address correspondence to
fcaruso@unimelb.edu.au,
ed.nice@monash.edu.

Received for review April 12, 2013
and accepted May 18, 2013.

Published online May 28, 2013
10.1021/nn401800u

© 2013 American Chemical Society

Such asymmetric distribution results in an unequal partitioning of key signaling molecules (*i.e.*, Notch and Delta) between two daughter cells, which may be pivotal in the maintenance of the stem cell niche. The understanding of how internalized particles redistribute when the original cell divides into two daughter cells is particularly important for proliferative cells, such as cancer cells, as cell division would lead to dilution of the intracellular particle concentration (and hence drug payload) during therapy. To date, few studies have reported on the distribution of particles during cell division despite the fact that many different types of nanoengineered particles have been generated. It has been shown that nanodiamonds⁹ and silica microparticles¹⁰ are equally distributed between two daughter cells, whereas, by contrast, the dilution of quantum dots^{11,12} upon cell division leads to asymmetric segregation. The different patterns of mitotic partitioning observed in such studies suggest that internalized particles, which have accumulated in the endocytic systems, may be further regulated during cell division. Investigations on the deterministic and stochastic mechanisms of particle partitioning are likely to shed light on the particle heterogeneity at the cell population level, providing a global landscape of cellular dynamics.

A number of polymer-based particle systems have been developed to facilitate drug solubility and improve drug pharmacokinetics, such as self-assembled polymersomes and micelles.¹³ Alternatively, templated assembly, which is a simple and versatile fabrication process, has emerged as a key approach in the preparation of polymer particles with well-defined and controllable physicochemical properties. This is exemplified by the development of a suite of polymer particles/capsules with controlled size, shape, and surface functionalization through layer-by-layer (LbL) assembly using nonporous particle templates.^{14,15} Templating porous particles, which involves polymers infiltrating the internal pore network, has yielded a new class of replica particles, termed nanoporous polymer particles (NPPs).^{16,17} Such polymer particles exhibit high cargo loading capacity due to their large surface area as a result of the porous templates. Mesoporous silica (MS) particles have been employed in the generation of a range of NPPs with different chemical composition, including polypeptides, synthetic polyelectrolytes, and polysaccharides.^{16,17}

Recently, progress has been made in applying NPPs for therapeutic delivery in a number of pathological scenarios.^{18–20} For example, nanoporous poly(L-glutamic acid) particles have been developed to deliver a brain-derived neurotrophic factor (BDNF) in an animal model to rescue neuronal cells that have lost their endogenous neurotrophin supply,¹⁸ while nanoporous poly(L-lysine) particles have been used to co-deliver a plasmid DNA and a peptide hormone for concurrent

stimulation of melanogenesis in mammalian melanocytes.¹⁹ An engineered drug-loaded particle system that combines drug-polymer conjugates and MS templating has also been developed.²⁰ These particles are prepared by infiltration of drug-conjugated thiolated poly(methacrylic acid) (PMA_{SH}) into submicrometer-sized MS particles, followed by subsequent oxidation of the thiol groups in the PMA_{SH} to form stable disulfide bonds, and dissolution of the silica templates. The resulting drug-loaded PMA_{SH} particles exhibit excellent monodispersity and are cytotoxic to colorectal cancer cells.²⁰ Given the simplicity of this approach, PMA_{SH} NPPs present an interesting therapeutic delivery particle system for biological applications. However, detailed studies on the cellular interactions of NPPs and subsequent particle partitioning during cancer cell division are yet to be performed.

Herein, we examine the cellular interactions, intracellular fate, mitotic partitioning, and cellular responses of PMA_{SH} NPPs. Our results show that these particles are effectively internalized by HeLa cells, traffic from early endosomes to lysosomes within a few minutes, and ultimately accumulate in the lysosomal compartments. Using both time-lapse and static fluorescence microscopy, we show that upon cell division, these lysosome-enclosed particles are distributed asymmetrically between two daughter cells. Additionally, proteomics techniques, based on 2D-DIGE and liquid chromatography coupled with tandem mass spectrometry (nano LC-MS/MS), have been used to elucidate potential underlying cellular mechanisms. We have identified 18 proteins that are differentially regulated. Importantly, all of these 18 proteins strongly align with the ubiquitylation network, suggesting a critical role of ubiquitylation in particle trafficking and sorting. Taken together, our data provide novel insights into cellular interactions of PMA_{SH} particles with respect to their intracellular trafficking and mitotic partitioning, which has implications in particle dynamics at both single cell and cell population levels.

RESULTS AND DISCUSSION

The PMA_{SH} NPPs used in this study were prepared as described previously²⁰ and were characterized by transmission electron microscopy (TEM), dynamic light scattering (DLS), and microelectrophoresis. These particles are monodisperse with an average diameter of 500 ± 50 nm (from TEM and DLS) (Figure 1a and b) and exhibit a zeta-potential of -38 mV. Subsequently, the particles were labeled with Alexa Fluor 633 (AF633) to allow qualitative and quantitative analyses using fluorescence-based techniques, including flow cytometry, imaging flow cytometry, and deconvolution microscopy. The cellular association of the particles was evaluated at a constant particle concentration (7.5×10^3 particles μL^{-1} ; particle-to-cell ratio of 100:1) as a function of time. It was shown that the percentage

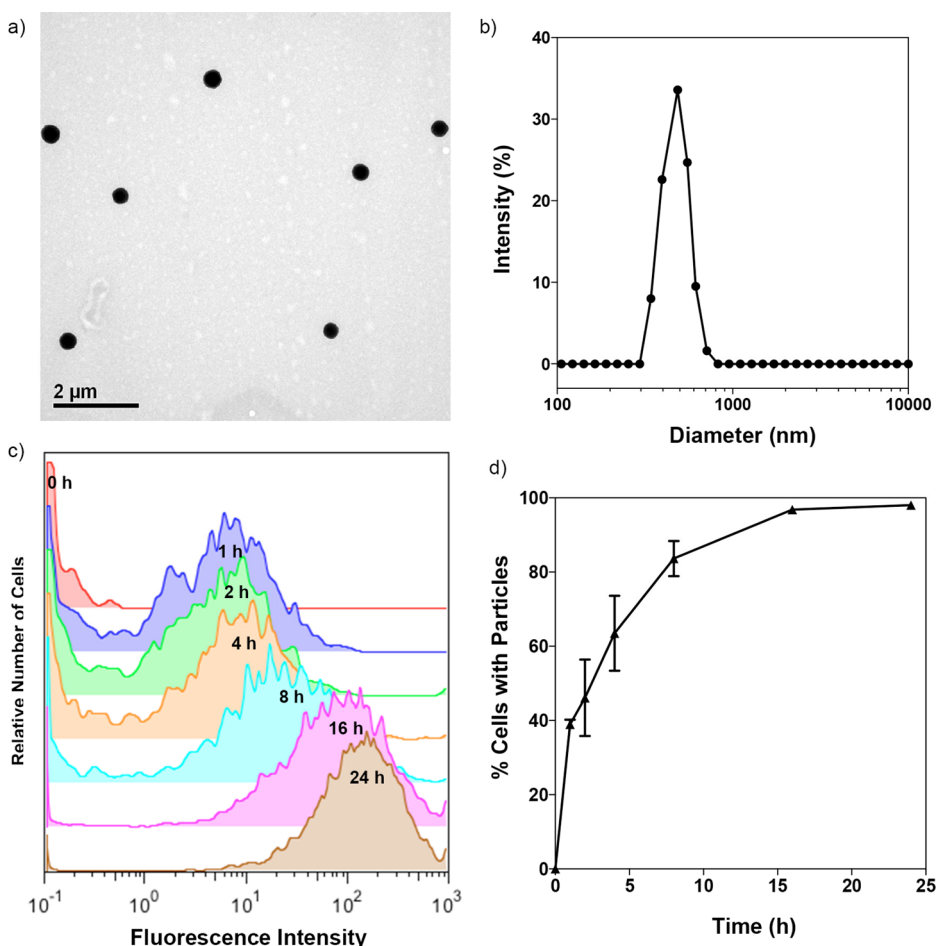


Figure 1. (a) TEM image of PMA_{SH} particles. (b) Size distribution of PMA_{SH} particles measured by DLS in 10 mM phosphate buffer, pH 7.4. (c) and (d) Time-dependent cellular association of AF633-labeled PMA_{SH} NPPs with HeLa cells: (c) Representative flow cytometry histograms showing the number of cells associated with particles and (d) percentage of cells with particles. Data are the mean \pm standard error of two independent experiments, and at least 10 000 cells were analyzed in each experiment. Flow cytometry analysis was performed after the cells were incubated with particles at a 100:1 particle-to-cell ratio over a 24 h incubation period at 37 °C and 5% CO₂.

of cells associated with the PMA_{SH} NPPs increased with incubation time and reached a plateau of \sim 95% at about 16 h (Figure 1c and d). On the basis of these cellular association kinetics, cells were incubated with PMA_{SH} particles for 24 h for subsequent internalization, intracellular fate, and mitotic partitioning analyses.

To quantitatively analyze the cellular uptake of the PMA_{SH} particles, imaging flow cytometry, which integrates flow cytometry and fluorescence imaging,²¹ was employed. Following treatment with the particles, cells were labeled with Vybrant CFDA SE Cell Tracer to mark the outline of the cells. By using the internalization feature in the IDEAS software, the probability of particle uptake was evaluated as an Internalization Score (IS). Based on the acquired images of the cells and the particles, the location of the particles in relation to the intracellular or extracellular space can be quantitatively analyzed by the IDEAS software. Cells with internalized particles give a positive IS. As shown in Figure 2, about 85% of cells with IS > 0 showed substantial uptake of the particles, which is consistent with previous reports

that submicrometer-sized PMA_{SH} capsules are readily internalized by a range of cells.^{21,22}

Next, we sought to acquire detailed information on the intracellular trafficking of the PMA_{SH} particles. In this study, we examined the subcellular destination of PMA_{SH} particles using deconvolution microscopy in both static and real-time modes. By co-transduction of HeLa cells with CellLight Early Endosomes-GFP and CellLight Lysosomes-RFP, we were able to track the mobility of the internalized PMA_{SH} particles between early endosomes and lysosomes. The live cell imaging showed that single particles were initially associated (vesicle fusion) with early endosomes, which encircled the internalized particles (Figure 3, frames 1 and 2). In the following 5 min, individual particles gradually disassociated (vesicle fission) from the early endosomes (Figure 3, frames 3 and 4). Ultimately, the particles increasingly co-localized with lysosomes (Figure 3, frames 5–12), indicating directed particle trafficking from early endosomes to lysosomes, which has also been observed for other nanoparticles.²³

This rapid trafficking of particles from early endosomes to lysosomes within a few minutes was observed in four independent time-lapse live cell experiments. An additional example where the trafficking between early endosomes to lysosomes was about 7.5 min is shown in Figure S1. The final intracellular distribution of the particles was further confirmed by immunostaining with the lysosomal marker LAMP1. As shown in Figure 4, the internalized PMA_{SH} NPPs exhibited strong co-localization with lysosomes in the cells that had been incubated with the particles for 24 h. Taken together, our data suggest that following internalization,

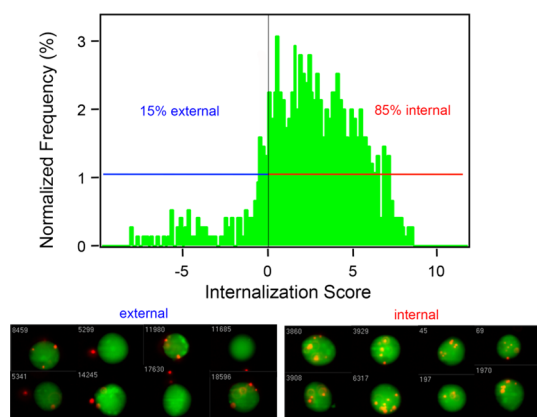


Figure 2. Quantification of the internalization of AF633-labeled PMA_{SH} particles in HeLa cells by imaging flow cytometry. Cells were incubated with particles at a particle-to-cell ratio of 100:1 for 24 h. Cells with internalized particles were selected by choosing the cell population with a positive internalization score. Representative images of cells with internalized particles (right panel) and cells with external surface-bound particles (left panel).

PMA_{SH} NPPs transiently fuse with early endosomes and ultimately accumulate in the lysosomes as their final intracellular destination after 24 h.

To examine the impact of the lysosome-trapped particles on mitosis, cell proliferation was evaluated using flow cytometry. Cells were incubated with PMA_{SH} particles at a particle-to-cell ratio of 100:1 for 24 h, followed by incubation in particle-free complete media for an additional 24 h. Viable cells were counted and compared with untreated cells at each time point. No significant changes in cell proliferation were observed (Figure S2), which is consistent with previous reports that PMA_{SH} particles have negligible cytotoxicity.²⁰ To understand the particle segregation following cell division at a single-cell resolution, the cell cycle was monitored by time-lapse imaging of cells subsequent to internalization of the PMA_{SH} particles. First, cells were transduced with CellLight Tubulin-GFP to labeled microtubules, allowing various phases of the cell cycle to be identified. AF633-PMA_{SH} particles were introduced into the cells by incubation for 24 h. After removal of excess particles, the cells were imaged for the following 24 h at 10 min intervals to monitor the cell cycle. A representative time-lapse series of a single HeLa cell undergoing mitosis is shown in Figure 5. Multiple particles were internalized by the cells and retained in various mitotic phases (prophase, metaphase, anaphase, and telophase) without disturbing spindle formation (Figure 5, upper and middle panels). Interestingly, during cytokinesis, the late stage of mitosis when the cytoplasm is divided into two daughter cells, the PMA_{SH} particles were asymmetrically segregated between the two cells (Figure 5, lower

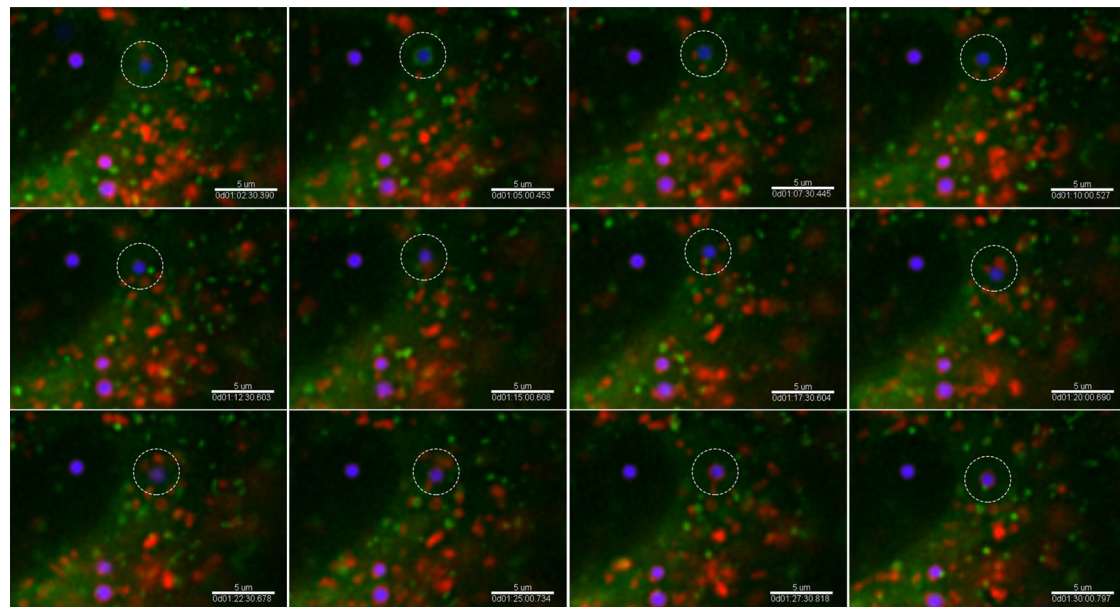


Figure 3. Intracellular trafficking of AF633-labeled PMA_{SH} particles in HeLa cells. Cells were transiently transduced with GFP-early endosomes (green) and RFP-lysosomes (red), and subsequently incubated with the PMA_{SH} particles (blue). Time-lapse deconvolution microscopy images were taken for 4 h following incubation with an interval of 2.5 min between sequential images. Scale bars = 5 μm.

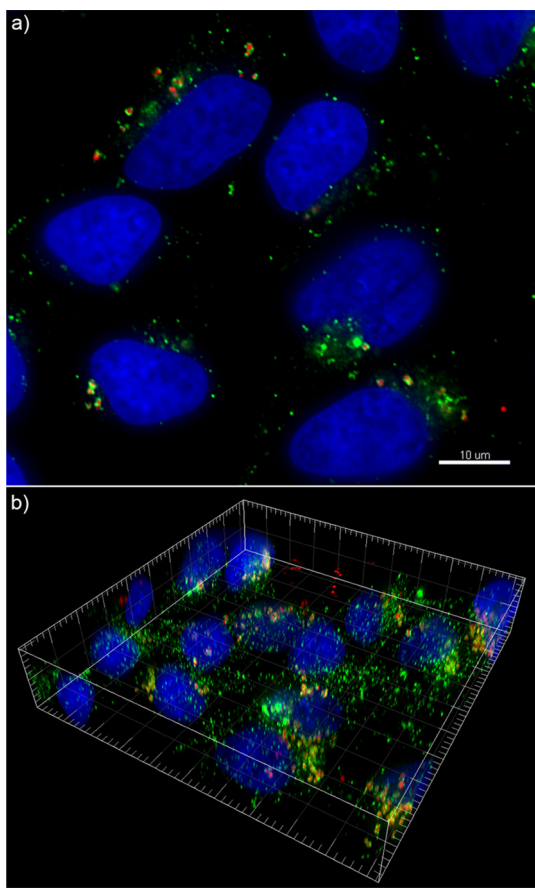


Figure 4. Intracellular distribution of AF633-labeled PMA_{SH} particles in HeLa cells. Cells were incubated with PMA_{SH} particles (red) for 24 h. Lysosomes were immunostained with anti-LAMP1 antibody (green), and nuclei were counterstained with Hoechst 33342 (blue). (a) Focal plane deconvolution microscopy image. Scale bar = 10 μm . (b) 3D deconvolution microscopy image. Axis tick = 1 μm .

panels). This asymmetric mitotic partitioning was observed in three independent time-lapse live cell experiments, and an additional example is shown in Figure S3.

To assess the population variation in mitotic partitioning of the particles, we sought to quantitatively evaluate the particle redistribution between the two daughter cells. After exposure to the particles for 24 h, cells were cultured in particle-free growth media for 20 h to allow them to continue through the cell cycle, as the mean division time for HeLa cells is 20.5 h.¹² This allows the cell population to progress through the cell cycle in the absence of the particles, which ensures that the particles observed in individual daughter cells were inherited from the parental cells. By immunostaining the microtubules with a mouse anti- α -tubulin monoclonal antibody, 152 cells undergoing cytokinesis were identified, and the number of particles in each daughter cell was determined.

In order to quantify the asymmetry, the segregation deviation (%) was calculated (see Methods for details). The frequency of segregation deviation was plotted

(Figure 6). This shows that the segregation deviation peaked at 60%, suggesting dilution of the lysosome-enclosed particles across cell generations is biased. Although the molecular mechanisms of lysosome inheritance are yet to be revealed, studies have suggested that endosomes and lysosomes are partitioned as intact vesicles.²⁴ Typically, lysosomes are accumulated in the vicinity of the microtubule organization center during cytokinesis and segregated into daughter cells by coordinated movements in a stochastic fashion.²⁴ Although several previous studies have shown that cell division results in a decrease in intracellular concentration of both nanodiamonds and silica microparticles by symmetrical dilution in two daughter cells,^{9,10} by contrast, studies on quantum dots have reported that partitioning during cell division is a random and asymmetric process, resulting in a faster dilution of quantum dots at the cell population level compared to symmetrical segregation.^{11,12} It has been suggested that the mitotic partitioning of internalized particles may be intimately connected to particle-induced cellular stress.¹² Consequently, asymmetrical division of particles may present a strategy to reduce the risk from an external toxin at the cell population level.¹²

Mass-spectrometry-based proteomics techniques have recently been demonstrated to be powerful tools for investigating cellular mechanisms and analyzing particle-induced cellular responses.²⁵ To identify differentially expressed proteins in response to PMA_{SH} NPP exposure for 24 h, 2D-DIGE and nano LC-MS/MS were employed to compare the overall changes between treated and untreated HeLa cells. Six cell culture replicates of each group were prepared (to allow statistical analysis²⁶). Half of each set was labeled with Cy3 and the other half with Cy5 DIGE label using a reverse labeling strategy.²⁶ Additionally, an internal control was prepared with equal volumes of each extract from both conditions and labeled with Cy2.²⁶ Randomly paired samples with opposite labeling and opposing conditions were mixed together with the internal control and separated on pH 3–10 nonlinear 24 cm IPG strips using cup loading, followed by separation on precast large-format 12.5% gels. Following the 2D separation, gels were scanned on a Typhoon scanner and the images analyzed using the DeCyder software package. Excellent reproducibly was noted between the six replicate gels (Figure S4). DeCyder analysis showed that, of the 3059 spots recognized on the gels, 127 spots were differentially regulated ($n = 6$, $p < 0.05$, data not shown). However, the level of change was typically relatively low (less than 2-fold). This is in agreement with our previous proteomics studies on cellular responses to nanoparticles, indicating that the changes induced were relatively subtle.²⁵ Following silver staining, 20 of the 127 differentially regulated spots were deemed suitably abundant for

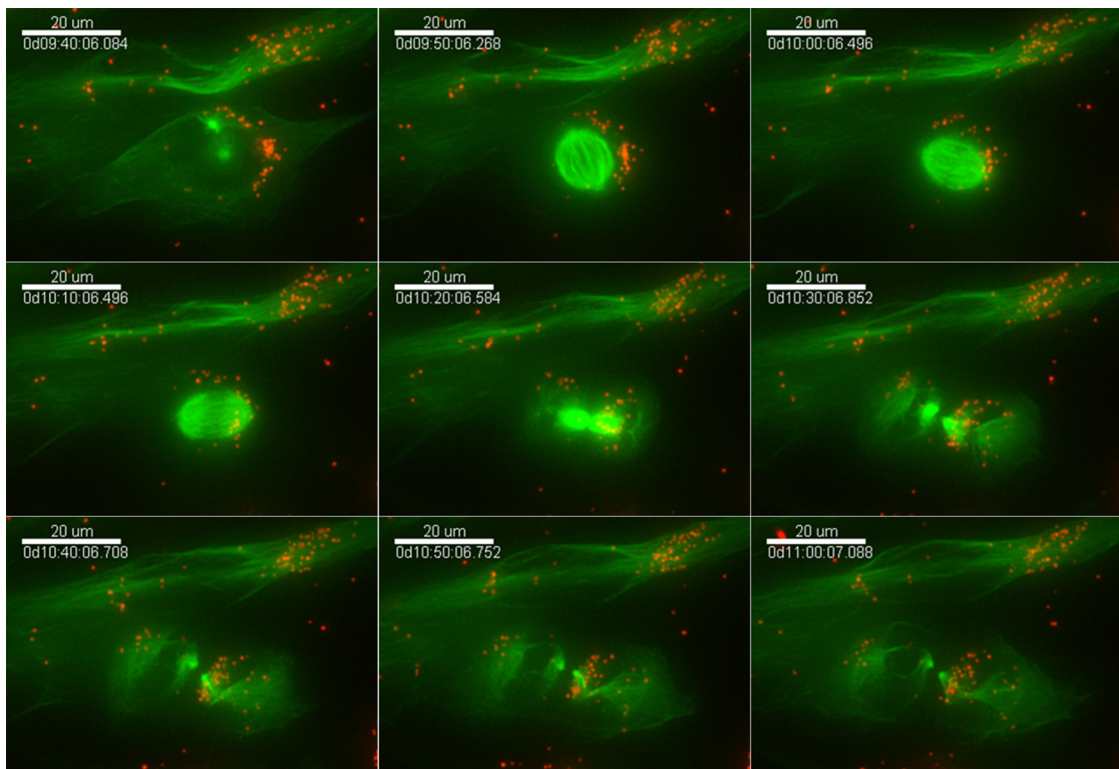


Figure 5. Distribution of AF633-labeled PMA_{SH} particles during mitosis. Cells were transiently transduced with GFE-tubulin (green) and incubated with the particles for 24 h. The following cell cycle was monitored by time-lapse deconvolution microscopy. Images were taken with an interval of 10 min for 24 h. Scale bars = 20 μ m.

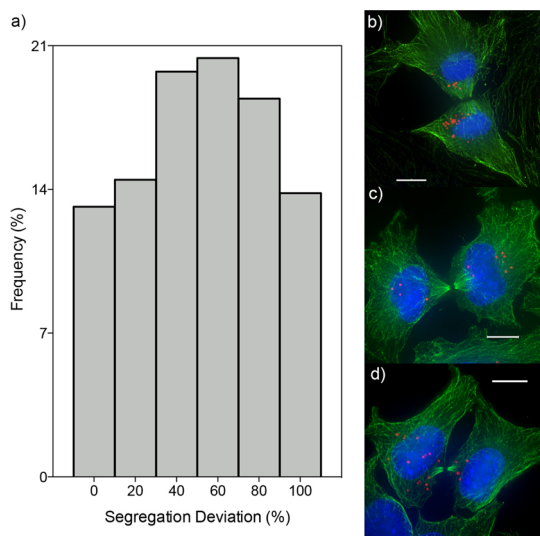


Figure 6. Quantitative analysis of mitotic partitioning of AF633-labeled PMA_{SH} particles in HeLa cells. Cells were incubated with the particles and immunostained with anti- α -tubulin monoclonal antibody. 152 cells in cytokinesis were identified, and the number of particles in daughter cells was determined. (a) Distribution of segregation deviation for 152 cells. Segregation deviation was calculated as the percentage of the difference to the sum of particles in both daughter cells. (b) Representative deconvolution microscopy images of cells undergoing cytokinesis. Microtubules are stained green, nuclei are labeled blue, and particles are shown in red. Scale bars = 10 μ m.

proteomics analysis. A landmark spot (spot 21, S4a) was taken as a reference point. All of these spots yielded interpretable data, and a total of 18 distinct proteins were identified from the major component(s) of each spot with multiple peptides corresponding to each protein identified (Table S1). Several proteins were identified in more than one gel spot, suggesting modifications or that different isoforms were detected.

Interestingly, 10 of these proteins (55.5%) (HNRNPL, EIF4A3, RPLPO, DLD, PKM2, VIM, HSPA8, HSPD1, HNRNPC, ENO1) had been previously identified in a meta-analysis of the 138 proteins reported in other proteomics-based analyses of cellular responses to nanoparticles on human cells,²⁵ confirming that, irrespective of the particle nature, a number of common pathways are regulated following particle uptake by cells.

Notably, 60S acidic ribosomal protein L0 (RPLP0) was identified in two adjacent spots (6 and 7, Figure S4a) of similar molecular weight but with different apparent isoelectric point (pI) values and expression moving in opposite directions, suggesting that either posttranslational modifications or different splicing isoforms were present. Though not definitive, dephosphorylation of RPLP0 following particle exposure is a strong possibility. Additionally, heterogeneous ribonucleoprotein C (HNRNPC) was identified in two spots (18 and 19,

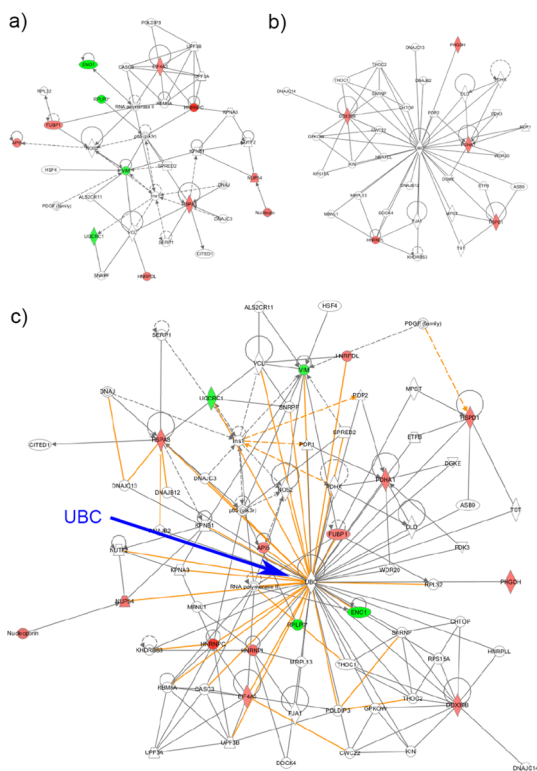


Figure 7. Protein network analysis of dysregulated proteins identified from 2D-DIGE MS/MS. Two standard networks were identified by IPA involved in functions of molecular transport (a and b), protein trafficking (a) and RNA trafficking (b). The merged network (c) highlights the central role of ubiquitin. Identified proteins are shown in red (up-regulated) and green (down-regulated) in response to particle treatment. Solid lines represent direct relationships. Dotted lines represent indirect relationships. Lines connecting the proteins indicate known inter-relationships from the IPA database. (An enlarged version of this figure is given in Figure S6.)

Figure S4a) with differing molecular weights. Both of these spots were among the most strongly upregulated in the DIGE analysis, with each displaying a similar increase in expression in particle-treated cells (1.62- and 1.72-fold, respectively). The peptides identified in the two spots clearly differentiated the alternative transcript/protein forms with an additional exon being present in the larger form (Figure S5).

Bioinformatics analysis using Ingenuity Pathway Analysis (IPA) software was performed to interpret the molecular networks and biological functions of the differentially regulated proteins (Figure 7; an enlarged form is provided in Figure S6). Twelve out of 18 of the proteins that we identified were clustered around a network involved in functions of molecular transport and protein trafficking (Figure 7a). While less well populated, five out of 18 of the proteins were ascribed a role in molecular transport and RNA trafficking (Figure 7b). Strikingly, the overlay of these two standard networks appeared to feed into the ubiquitylation network (Figure 7c). Traditionally, ubiquitylation has been regarded as a protein degradation mechanism by reversibly modifying proteins with

ubiquitin and subsequently directing them to the proteasome.²⁷ More recently, evidence has demonstrated that ubiquitylation also plays critical roles in nonproteolytic functions, such as endocytosis.²⁸ For example, the addition of single ubiquitin moieties to epidermal growth factor receptor (EGFR) cytoplasmic tail induces its internalization and trafficking to lysosomes.²⁹ Further, ubiquitylation of cell membrane receptors of several viruses, such as the influenza virus³⁰ and herpes simplex virus,³¹ is required for virus entry and trafficking. In particular, the balance between ubiquitylation and deubiquitylation has been suggested to govern the efficiency of recycling from endosomes to the plasma membrane *versus* lysosomal sorting through the multivesicular body pathway.²⁸ The role of ubiquitylation and lysosomal accumulation observed in this study, suggesting little recycling of the particles following internalization, supports the findings of negligible exportation of nanoparticles reported previously.³² Taken together, the proteomics data demonstrate that ubiquitylation activities are the major cellular responses to the particles, suggesting the central role of ubiquitylation in regulating the particle uptake and trafficking. Clearly, we are only at the beginning of understanding the ubiquitylation functions in the cell–particle interactions, and more work will be needed to further examine the proteome and identify the cellular proteins that are specifically and reversibly modified in response to the PMA_{SH} NPPs.

CONCLUSIONS

The present study provides the first investigation of cellular interactions as well as cellular regulatory networks of PMA_{SH} NPPs that are being developed for biological applications. The interactions between the PMA_{SH} NPPs and HeLa cells have been qualitatively and quantitatively characterized using various techniques, including fluorescence imaging and proteomics. Our data have shown that the particles rapidly traffic from early endosomes to lysosomes following internalization, which occurs over a few minutes. Using both static and time-lapse imaging modes, this study provides quantitative evidence that the internalized particles are partitioned asymmetrically between two daughter cells upon cell division. The biased segregation of particles gives rise to daughter cells that differ in particle dose, providing valuable information on the heterogeneity of particle inheritance. Furthermore, the proteomic analysis has identified a number of differentially expressed proteins upon exposure to the PMA_{SH} NPPs to HeLa cells and suggests that ubiquitylation is a key signal triggered by the particles. It is also noted that the intracellular mobility of particles is strongly influenced by particle size, shape, and surface chemistry, as well as cell physiology. Hence, future studies will be aimed at identifying the physicochemical properties of particles that govern cellular

processing.^{33,34} Nonetheless, the reported findings shed light on the mechanisms that govern the cellular journey of the PMA_{SH} particles, from trafficking to inheritance. Understanding the intrinsic regulatory

networks of the particles will be key to evaluating their efficacy and safety for their biological applications, and potentially allowing control of particle internalization, trafficking, and localization at subcellular levels.

METHODS

Materials. Poly(methacrylic acid, sodium salt) (PMA, M_w 15 kDa) was purchased from Polysciences (USA). N-Chloro-p-toluenesulfonamide sodium salt (chloramine T), hydrofluoric acid (HF), dithiothreitol (DTT), sodium citrate dihydrate, 1-pentanol tetraethyl orthosilicate (TEOS), N-(3-dimethylaminopropyl)-N'-ethylcarbodiimide hydrochloride (EDC), (3-aminopropyl)-triethoxysilane (APTES), and phosphate-buffered saline were purchased from Sigma-Aldrich and used as received. 3-(N-Morpholino)propanesulfonic acid (MES) was obtained from Acros Organics. Sodium acetate (NaOAc), 2-(N-morpholine)ethanesulfonic acid, and ammonia were purchased from Merck. Pyridine dithioothiamine hydrochloride was obtained from Shanghai Speed Chemical Co. Ltd., China. Alexa Fluor 488 goat anti-mouse IgG, Alexa Fluor 633 hydrazide (AF633) reactive dyes, Dulbecco's modified Eagle's medium (DMEM), GlutaMax, heat-inactivated fetal bovine serum (HI-FBS), Dulbecco's phosphate-buffered saline (DPBS), CO₂-independent medium, CellLight Early Endosomes-GFP, CellLight Lysosomes-RFP, CellLight Tubulin-GFP, and Hoechst 33342 were purchased from Life Technologies. Mouse anti- α -tubulin monoclonal antibody (clone B-5-1-2) was purchased from Sigma-Aldrich. Mouse anti-human LAMP1 monoclonal antibody (clone H4A3) was purchased from BD Pharmingen. Ultrapure water with resistance greater than 18 M Ω cm was obtained from an inline Millipore RiOs/Origin system (Millipore Corporation, USA).

Preparation of PMA_{SH} Particles. PMA_{SH} with 20% thiol modification and PMA_{SH} particles were prepared using our previously reported protocols.²⁰ Briefly, approximately 3 mg of APTES-modified MS particles was dispersed in 5 mg mL⁻¹ of PMA_{SH} solution at pH 4.5 (600 μ L of NaOAc buffer, 50 mM) under constant shaking overnight. Subsequently, the particles were isolated by centrifugation and washed twice with NaOAc buffer. The pellet was dispersed in 50 μ L of NaOAc buffer and exposed to a 10 mM solution of chloramine T in MES buffer (pH 6, 50 mM) for 2 min. After two washing cycles with water, the MS templates were dissolved with a 2 M HF/8 M NH₄F solution (pH ~5). *Caution! HF is highly toxic. Extreme care should be taken when handling HF solution and only small quantities should be prepared.* The resultant PMA_{SH} particles were washed three times with water and labeled with AF633 via EDC-mediated amide bond formation between the carboxyl groups of PMA and hydrazide groups of AF633 in DPBS buffer. The fluorescently labeled PMA_{SH} particles were counted using a CyFlow Space (Partec GmbH) flow cytometer with 488 and 633 nm lasers, as reported previously.³⁴ The flow cytometer counts the particle number based on the particle fluorescence and scattering signals in the known volume.

Cell Culture. HeLa cells were maintained in DMEM media with the addition of 1% (v/v) GlutaMax and 10% (v/v) HI-FBS at 37 °C in a 5% CO₂ humidified atmosphere and subcultured prior to confluence using trypsin.

Cellular Association Analysis. HeLa cells were plated at a density of 7.5×10^4 cells per well into 24-well plates and allowed to adhere overnight. Cells were then incubated with AF633-labeled PMA_{SH} particles at a capsule-to-cell ratio of 100:1 for different time intervals in a total volume of 1 mL complete growth DMEM media (37 °C, 5% CO₂). After treatment, the cells were washed with DPBS three times and harvested by trypsinization and centrifugation at 400g for 5 min. The cell pellet was resuspended in DPBS and analyzed by flow cytometry. Flow cytometry analysis was performed using a CyFlow Space (Partec GmbH) flow cytometer using lasers with excitation wavelengths of 488 and 633 nm. In each measurement at least 10 000 cells were analyzed.

Internalization Analysis by Imaging Flow Cytometry. Cells treated with particles were prepared as described above. Briefly, 9×10^5

cells were seeded into T25 flasks and treated with AF633-labeled PMA HCs at a capsule-to-cell ratio of 100:1 for 24 h in complete growth DMEM media. After the treatment, the cells were washed with DPBS three times. Cells were further labeled with Vybrant CFDA SE Cell Tracer (0.5 μ M) according to the manufacturer's protocol. Cells were subsequently trypsinized and collected by centrifugation at 400g for 5 min. Cold DPBS was used to resuspend cells and keep them on ice until analysis using imaging flow cytometry. Images of 5000 cells and the capsule fluorescence intensities were acquired. The internalization analysis was performed using the built-in internalization feature of IDEAS software on single focused cells associated with capsules.

Intracellular Fate of PMA_{SH} Particles by Deconvolution Microscopy.

HeLa cells were plated at 3×10^4 cells per well into eight-well Lab-Tek I chambered coverglass slides (Thermo Fisher Scientific, Rochester, NY, USA) and allowed to adhere overnight. The cells were then incubated with AF633-labeled PMA_{SH} particles at a capsule-to-cell ratio of 100:1 for 24 h in complete growth DMEM media (37 °C, 5% CO₂). Following this, the cells were washed with DPBS three times and fixed with 4% paraformaldehyde for 30 min at room temperature (RT) of 22 °C and permeabilized with 0.1% Triton X-100 in DPBS for 5 min at RT. Lysosomes were immunostained with anti-LAMP1 antibody (2.5 μ g mL⁻¹) and AF488-goat anti-mouse IgG (2 μ g mL⁻¹). Nuclei were counterstained with Hoechst 33342 (2 μ g mL⁻¹). Fluorescence images and optical sections were collected using a deconvolution microscope (DeltaVision, Applied Precision). Images were processed with Imaris 6.3.1 software (Bitplane).

Live Cell Time Lapse Imaging. HeLa cells were plated at 1.5×10^4 cells per well into eight-well Lab-Tek I chambered coverglass slides (Thermo Fisher Scientific, Rochester) and allowed to adhere overnight. The cells were then incubated with CellLight Early Endosomes-GFP, CellLight Lysosomes-RFP, or CellLight Tubulin-GFP to label early endosomes, lysosomes, or microtubulin, respectively. The cells were transduced at a ratio of cell-to-baculovirus of 1:30 and incubated for 24 h before imaging. Following the transduction, fresh complete DMEM media containing AF633-labeled PMA_{SH} particles (1.5×10^6 particles/chamber) were added. After the treatment, fresh CO₂-independent media with the addition of 1% GlutaMax and 10% HI-FBS were added. Time-lapse fluorescence images and optical sections were collected using deconvolution microscopy for a total of 4 h with 2.5 min intervals to image intracellular trafficking or for a total of 24 h with 10 min intervals to image cell division. The acquired movies were processed with Imaris 6.3.1 software (Bitplane).

Imaging of Cytokinesis. HeLa cells were plated at 1.5×10^4 cells per well into eight-well Lab-Tek I chambered coverglass slides and allowed to adhere overnight. The cells were then incubated with AF633-labeled PMA_{SH} particles (1.5×10^6 particles/chamber) for 24 h in complete growth DMEM media. The treatment media was then replaced with fresh complete DMEM media, and the cells were cultured for an additional 20 h. The cells were subsequently fixed with 4% paraformaldehyde and permeabilized with 0.1% Triton X-100 for 5 min at RT. The cells were then immunostained with anti- α -tubulin monoclonal antibody (1:2000 dilution in DPBS containing 1% BSA) and AF488-goat anti-mouse IgG (2 μ g mL⁻¹). Nuclei were counterstained with Hoechst 33342 (2 μ g mL⁻¹). Fluorescence images and optical sections were collected using a deconvolution microscope (DeltaVision, Applied Precision). 152 cells undergoing cytokinesis were identified on the basis of the characteristic structure of microtubules. The particles distributed between two daughters were counted using the particle-counting function of the Imaris 6.3.1 software (Bitplane). The segregation

deviation (%) was calculated as follows: $(B - A)/(B + A) \times 100$, where B and A represent the number of particles for two daughter cells ($B \geq A$). The frequency of segregation deviation was plotted using Prism 5 software (GraphPad).

Proteomic Analysis Using 2D-DIGE. Harvested cells from six biological replicates of untreated and particles treated with HeLa cells were lysed in RIPA buffer containing the proteolytic inhibitors Aprotinin (100 $\mu\text{g mL}^{-1}$), Leupeptin (500 $\mu\text{g mL}^{-1}$), and Pepstatin A (70 $\mu\text{g mL}^{-1}$) (American Bioanalytical) for 4 h at 4 °C. Protein concentrations of cell lysates were determined using a 2-D Quant Kit (GE Healthcare) according to the manufacturer's instructions. Subsequently, protein (100 μg) was precipitated using a 2-D Clean-Up Kit (GE Healthcare) according to the manufacturer's instructions. Proteins were then dissolved in 7 M urea, 2 M thiourea, 4% (w/v) CHAPS, and 30 mM Tris-HCl pH 8.5. Labeling reactions were performed in a 45 μL volume with 30 μg of the protein lysates, in the presence of 400 pmol of Cy2-, Cy3-, or Cy5-dyes (minimal labeling dyes, GE Healthcare), by implementation of a dye-swapping strategy.³⁵ Three extracts from untreated HeLa cells were labeled with Cy3, while three extracts from cells that had been treated with particles were labeled with Cy5. In a complementary manner, three extracts of untreated cells were labeled with Cy5, and three extracts of cells treated with particles were labeled with Cy3. Six mixtures of the paired samples (30 μg each) were also labeled with Cy2 dye, the internal standard used for the 2D-DIGE procedure. The labeling was performed for 30 min on ice, in the dark, and chased with 1 mM lysine. Six sample mixtures, made of appropriate Cy3- and Cy5-labeled pairs and a Cy2-labeled control, were supplemented with 1% v/v IPG buffer, pH 3–10 NL (GE Healthcare), 1.4% v/v DeStreak reagent (GE Healthcare), and 0.2% w/v DTT to a final volume of 300 μL in 7 M urea, 2 M thiourea, and 4% CHAPS. The mixtures (90 μg of total protein content) were used for passive hydration of immobilized pH gradient IPG gel strips (24 cm, pH 3–10 NL) for 16 h at 20 °C. Isoelectric focusing was performed on an IPGphor II apparatus (GE Healthcare) up to 8000 V h⁻¹ at 20 °C (current limit, 50 $\mu\text{A}/\text{strip}$). The strips were equilibrated in 6 M urea, 2% SDS, 20% glycerol, and 0.375 M Tris-HCl (pH 8.8) for 15 min, in the presence of 0.5% w/v DTT, and then in the presence of 4.5% w/v iodoacetamide in the same buffer for an additional 15 min in the dark. The equilibrated IPG strips were finally transferred onto 4–20% polyacrylamide gels, within low-fluorescence glass plates (ETTAN-DALT 6 system, GE Healthcare). The second-dimension SDS-PAGE was performed on a DALT II electrophoresis unit (GE Healthcare) at 1 W/gel for 16 h. Gels were scanned on a Typhoon 9400 variable mode imager (GE Healthcare), with the indicated excitation/emission wavelengths for Cy2 (488/520 nm), Cy3 (532/580 nm), and Cy5 (633/670 nm) with a pixel size of 100 μm . Images were acquired with the ImageQuant software (GE Healthcare) and analyzed using the DeCyder 6.0 software (GE Healthcare). A DeCyder differential in-gel-analysis module was used for spot detection and pairwise comparison of each sample (Cy3 and Cy5) to the Cy2 mixed standard present in each gel. The DeCyder biological variation analysis (BVA) module was then used to simultaneously match all of the protein-spot maps from the gels and to calculate average abundance ratios and *P* values across the six replicate sets of samples (Student's *t* test). After spot matching with the master gel from the analytical step in the BVA module of DeCyder software, 2D gels were silver stained and spots picked for in-gel tryptic digest and MS analysis. Excised gel spots were digested as previously described³⁶ using iodoacetamide for cysteine alkylation. Digested protein spot extracts were loaded onto an Ultimate 3000 UPLC (Dionex, Thermo Scientific) fitted with a nanotrap column (Acclaim PepMap100 C₁₈, 100 μm i.d. \times 2 cm, 5 μm , 100 Å) at 10 $\mu\text{L min}^{-1}$ in 5% buffer B. Peptides were then resolved on an Acclaim PepMap RSLC C₁₈ column (75 μm i.d. \times 15 cm, 2 μm , 100 Å) at 300 nL min⁻¹ using a 30 min gradient from 5 to 55% buffer B (buffer A: 0.1% formic acid, buffer B: 95% acetonitrile/0.1% formic acid). The column was maintained at 40 °C. The column eluate was connected online to a QExactive mass spectrometer (Thermo) through a nanoelectrospray source. Parent ion scans (350–2000 m/z , 70 k resolution, AGC target 1e6, 60 ms max ion time) were used to select up to 10 multiply charged ions to subject to MS/MS (17.5 k resolution, AGC

target 5e5, 120 ms maximum ion time, isolation width 2.5 m/z , NCE 28.0) using an intensity threshold of 1.3e5 (underfill ratio of 3%). Dynamic exclusion was employed for 15 s. Spectra were converted to mzXML format using MSConvert (ProteoWizard version 3.0.3631). Spectra were searched using X!Tandem through gpm-xe manager (version 2.2.1) against human proteins from Ensembl (build GRCh37.64, with reversed sequences). Search parameters included trypsin cleavage specificity, fixed cysteine carbamidomethylation, variable methionine oxidation, parent mass accuracy 20 ppm, fragment mass accuracy 50 ppm, and one missed cleavage.

Pathway Analysis. The list of regulated proteins identified by 2D-DIGE/MS was analyzed by pathway analysis using the network-building tool Ingenuity Pathway Analysis (IPA) (Ingenuity Systems, www.ingenuity.com). IPA combines the currently available data for gene, protein, chemical, normal cellular and disease processes, signaling, and metabolic pathways to generate interaction networks. Significance was measured using Fisher's *t*-test, which relies on *p*-values to determine whether the null hypothesis should be accepted or rejected. Molecular functions with a *p*-value < 0.01 were considered significant.

Conflict of Interest: The authors declare no competing financial interest.

Acknowledgment. This work was supported by the Australian Research Council under the Australian Laureate Fellowship (F.C., FL120100030) and Discovery Early Career Researcher Award (Y.Y., DE130100488) schemes and by the National Health and Medical Research Council (NHMRC) Program Grant 487922 (F.C.).

Supporting Information Available: Time-lapse images of PMA_{SH} NPP intracellular trafficking, cell viability following exposure to PMA_{SH} particles, time-lapse images of PMA_{SH} NPP mitotic partitioning, 2D-DIGE, table of differentially expressed proteins identified, and alignments of protein sequences from spots 18 and 19. This material is available free of charge via the Internet at <http://pubs.acs.org>.

REFERENCES AND NOTES

- Yan, Y.; Such, G. K.; Johnston, A. P. R.; Best, J. P.; Caruso, F. Engineering Particles for Therapeutic Delivery: Prospects and Challenges. *ACS Nano* **2012**, *6*, 3663–3669.
- Canton, I.; Battaglia, G. Endocytosis at the Nanoscale. *Chem. Soc. Rev.* **2012**, *41*, 2718–2739.
- Duncan, R.; Richardson, S. C. W. Endocytosis and Intracellular Trafficking as Gateways for Nanomedicine Delivery: Opportunities and Challenges. *Mol. Pharm.* **2012**, *9*, 2380–2402.
- Marsh, M.; McMahon, H. T. The Structural Era of Endocytosis. *Science* **1999**, *285*, 215–220.
- Scita, G.; Di Fiore, P. P. The Endocytic Matrix. *Nature* **2010**, *463*, 464–473.
- Doherty, G. J.; McMahon, H. T. Mechanisms of Endocytosis. *Annu. Rev. Biochem.* **2009**, *78*, 857–902.
- Andrews, R.; Ahringer, J. Asymmetry of Early Endosome Distribution in *C. elegans* Embryos. *PLoS One* **2007**, *2*, e493.
- Beckmann, J.; Scheitz, S.; Wernet, P.; Fischer, J. C.; Giebel, B. Asymmetric Cell Division within the Human Hematopoietic Stem and Progenitor Cell Compartment: Identification of Asymmetrically Segregating Proteins. *Blood* **2007**, *109*, 5494–5501.
- Liu, K.-K.; Wang, C.-C.; Cheng, C.-L.; Chao, J.-I. Endocytic Carboxylated Nanodiamond for the Labeling and Tracking of Cell Division and Differentiation in Cancer and Stem Cells. *Biomaterials* **2009**, *30*, 4249–4259.
- Serda, R. E.; Ferrati, S.; Godin, B.; Tasciotti, E.; Liu, X.; Ferrari, M. Mitotic Trafficking of Silicon Microparticles. *Nanoscale* **2009**, *1*, 250–259.
- Errington, R. J.; Brown, M. R.; Silvestre, O. F.; Njoh, K. L.; Chappell, S. C.; Khan, I. A.; Rees, P.; Wilks, S. P.; Smith, P. J.; Summers, H. D. Single Cell Nanoparticle Tracking to Model Cell Cycle Dynamics and Compartmental Inheritance. *Cell Cycle* **2010**, *9*, 121–130.

12. Summers, H. D.; Rees, P.; Holton, M. D.; Brown, M. R.; Chappell, S. C.; Smith, P. J.; Errington, R. J. Statistical Analysis of Nanoparticle Dosing in a Dynamic Cellular System. *Nat. Nanotechnol.* **2011**, *6*, 170–174.
13. Mai, Y.; Eisenberg, A. Self-Assembly of Block Copolymers. *Chem. Soc. Rev.* **2012**, *41*, 5969–5985.
14. Yan, Y.; Such, G. K.; Johnston, A. P. R.; Lomas, H.; Caruso, F. Toward Therapeutic Delivery with Layer-by-Layer Engineered Particles. *ACS Nano* **2011**, *5*, 4252–4257.
15. De Koker, S.; Hoogenboom, R.; De Geest, B. G. Polymeric Multilayer Capsules for Drug Delivery. *Chem. Soc. Rev.* **2012**, *41*, 2867–2884.
16. Wang, Y.; Angelatos, A. S.; Caruso, F. Template Synthesis of Nanostructured Materials via Layer-by-Layer Assembly. *Chem. Mater.* **2008**, *20*, 848–858.
17. Wang, Y.; Price, A. D.; Caruso, F. Nanoporous Colloids: Building Blocks for a New Generation of Structured Materials. *J. Mater. Chem.* **2009**, *19*, 6451–6464.
18. Tan, J.; Wang, Y.; Yip, X.; Glynn, F.; Shepherd, R. K.; Caruso, F. Nanoporous Peptide Particles for Encapsulating and Releasing Neurotrophic Factors in an Animal Model of Neurodegeneration. *Adv. Mater.* **2012**, *24*, 3362–3366.
19. Zhang, X.; Oulad-Abdelghani, M.; Zelkin, A. N.; Wang, Y.; Haikel, Y.; Mainard, D.; Voegel, J.-C.; Caruso, F.; Benkirane-Jessel, N. Poly(L-lysine) Nanostructured Particles for Gene Delivery and Hormone Stimulation. *Biomaterials* **2010**, *31*, 1699–1706.
20. Cui, J.; Yan, Y.; Wang, Y.; Caruso, F. Templated Assembly of pH-Labile Polymer-Drug Particles for Intracellular Drug Delivery. *Adv. Funct. Mater.* **2012**, *22*, 4718–4723.
21. Yan, Y.; Johnston, A. P. R.; Dodds, S. J.; Kamphuis, M. M. J.; Ferguson, C.; Parton, R. G.; Nice, E. C.; Heath, J. K.; Caruso, F. Uptake and Intracellular Fate of Disulfide-Bonded Polymer Hydrogel Capsules for Doxorubicin Delivery to Colorectal Cancer Cells. *ACS Nano* **2010**, *4*, 2928–2936.
22. De Rose, R.; Zelikin, A. N.; Johnston, A. P. R.; Sexton, A.; Chong, S.-F.; Cortez, C.; Mulholland, W.; Caruso, F.; Kent, S. J. Binding, Internalization, and Antigen Presentation of Vaccine-Loaded Nanoengineered Capsules in Blood. *Adv. Mater.* **2008**, *20*, 4698–4703.
23. Schweiger, C.; Hartmann, R.; Zhang, F.; Parak, W. J.; Kissel, T. H.; Rivera-Gil, P. Quantification of the Internalization Patterns of Superparamagnetic Iron Oxide Nanoparticles with Opposite Charge. *J. Nanobiotechnol.* **2012**, *10*, 28.
24. Bergeland, T.; Widerberg, J.; Bakke, O.; Nordeng, T. W. Mitotic Partitioning of Endosomes and Lysosomes. *Curr. Biol.* **2001**, *11*, 644–651.
25. Lai, Z. W.; Yan, Y.; Caruso, F.; Nice, E. C. Emerging Techniques in Proteomics for Probing Nano–Bio Interactions. *ACS Nano* **2012**, *6*, 10438–10448.
26. Beckett, P. The Basics of 2D DIGE. *Methods Mol. Biol.* **2012**, *854*, 9–19.
27. Hicke, L. Protein Regulation By Monoubiquitin. *Nat. Rev. Mol. Cell Biol.* **2001**, *2*, 195–201.
28. Clague, M. J.; Liu, H.; Urbé, S. Governance of Endocytic Trafficking and Signaling by Reversible Ubiquitylation. *Dev. Cell* **2012**, *23*, 457–467.
29. Marmor, M. D.; Yarden, Y. Role of Protein Ubiquitylation in Regulating Endocytosis of Receptor Tyrosine Kinases. *Oncogene* **2004**, *23*, 2057–2070.
30. Khor, R.; McElroy, L. J.; Whittaker, G. R. The Ubiquitin-Vacuolar Protein Sorting System Is Selectively Required during Entry of Influenza Virus into Host Cells. *Traffic* **2003**, *4*, 857–868.
31. Delboy, M. G.; Roller, D. G.; Nicola, A. V. Cellular Proteasome Activity Facilitates Herpes Simplex Virus Entry at a Post-penetration Step. *J. Virol.* **2008**, *82*, 3381–3390.
32. Kim, J. A.; Åberg, C.; Salvati, A.; Dawson, K. A. Role of Cell Cycle on the Cellular Uptake and Dilution of Nanoparticles in A Cell Population. *Nat. Nanotechnol.* **2011**, *7*, 62–68.
33. Albanese, A.; Tang, P. S.; Chan, W. C. The Effect of Nanoparticle Size, Shape, and Surface Chemistry on Biological Systems. *Annu. Rev. Biomed. Eng.* **2012**, *14*, 1–16.
34. Shimon, O.; Yan, Y.; Wang, Y.; Caruso, F. Shape-Dependent Cellular Processing of Polyelectrolyte Capsules. *ACS Nano* **2013**, *7*, 522–530.
35. Karp, N. A.; Kreil, D. P.; Lilley, K. S. Determining a Significant Change in Protein Expression with DeCyder during a Pair-Wise Comparison Using Two-Dimensional Difference Gel Electrophoresis. *Proteomics* **2004**, *4*, 1421–1432.
36. Shevchenko, A.; Tomas, H.; Havlis, J.; Olsen, J. V.; Mann, M. In-Gel Digestion for Mass Spectrometric Characterization of Proteins and Proteomes. *Nat. Protoc.* **2007**, *1*, 2856–2860.